

## Article

# A Case Study on the Closed-Type Barrier Effect on Debris Flows at Mt. Woomyeon, Korea in 2011 via a Numerical Approach

Shin-Kyu Choi and Tae-Hyuk Kwon \* 

Department of Civil and Environmental Engineering, Korea Advanced Institute of Science and Technology, Daejeon 34141, Korea; newsk@kaist.ac.kr

\* Correspondence: t.kwon@kaist.ac.kr

**Abstract:** Debris flows are capable of flowing with high velocities and causing significant economic and infrastructural damage. As a hazard mitigation measure, physical barriers are frequently installed to dissipate the energy of debris flows. However, there is a lack of understanding on how barriers affect and interact with debris-flow behavior (e.g., velocity and volume). This study investigated the changes in debris-flow characteristics depending on the installation location of barriers. Mt. Woomyeon, which is located in Seoul, Korea, was the site of a major debris-flow event in 2011. This study modeled this event using DAN3D, numerical software based on smoothed particle hydrodynamics (SPH). Our numerical approach assessed changes in debris-flow behavior, including velocity and volume, as the debris flow interacts with four closed-type barriers installed at separate points along the flow path. We used DAN3D to model the barriers via terrain elevation modifications. The presence of a closed-type barrier results in the reduction in the debris-flow velocity and volume compared to when no barrier is present. Most notably, the closer a barrier is installed to the debris source, the greater the velocity decrease. By contrast, a barrier that is constructed further downstream allows the debris flow to undergo entrainment-driven growth before confronting the barrier, resulting in a larger debris deposition volume that can often cause overflow, as shown at our particular study site. The presented results highlight the effectiveness of barriers as a method of hazard mitigation by providing insight into how such installations can alter debris-flow behavior. In addition, the findings can provide a reference for future debris-flow barrier designs, increasing the effectiveness and efficiency of such barrier systems.

**Keywords:** debris flow; closed-type barrier; barrier location; barrier capacity



**Citation:** Choi, S.-K.; Kwon, T.-H. A Case Study on the Closed-Type Barrier Effect on Debris Flows at Mt. Woomyeon, Korea in 2011 via a Numerical Approach. *Energies* **2021**, *14*, 7890. <https://doi.org/10.3390/en14237890>

Academic Editor: Joel Sarout

Received: 22 October 2021

Accepted: 23 November 2021

Published: 24 November 2021

**Publisher's Note:** MDPI stays neutral with regard to jurisdictional claims in published maps and institutional affiliations.



**Copyright:** © 2021 by the authors. Licensee MDPI, Basel, Switzerland. This article is an open access article distributed under the terms and conditions of the Creative Commons Attribution (CC BY) license (<https://creativecommons.org/licenses/by/4.0/>).

## 1. Introduction

A debris flow is a phenomenon that involves the initiation of a landslide on a steep slope, the rapid flow of debris along a confined channel, and the eventual deposition of its contents on a flat area. Debris flows are considered as the most hazardous type of landslide due to their poor predictability and devastating destruction associated with their fast flow velocity, large impact forces, and long run-out distances [1]. In China, hundreds of channelized debris flows were triggered by heavy rainfall on 12–14 August 2010 [2]. The debris-flow event in the Hongchun gully was one of the most disastrous incidents in terms of scale. Here, the initial source volume of 183,000 m<sup>3</sup> grew to 700,000–800,000 m<sup>3</sup> as the debris flow moved downstream. The entrained debris blocked the Mingjiang River at the outlet of the gully, resulting in 17 casualties [3]. In the Southern Leyte Province, Philippines, a large-scale landslide caused by heavy rainfall inundated a village and covered about 500 houses and a school building on 17 February 2006. The debris flow mobilized boulders and debris totaling a volume of 10–15 million m<sup>3</sup>, resulting in 1149 casualties [4]. On 26–27 July 2011, 151 landslides and 33 debris flows took place at Mt. Woomyeon, Seoul, Korea [5]. The majority of the debris was deposited on the lower reaches of Mt. Woomyeon, where many local communities are located. This event caused 16 casualties and incurred an

enormous financial cost of approximately USD 15 million. In particular, some of the debris surged to the third floor of an apartment with a velocity of 28.6 m/s, as estimated from videos taken by residents [5,6].

Debris-flow barriers have been widely used as a countermeasure to reduce the damage caused by debris flows through energy dissipation and relevant hazard mitigation. Many research efforts have been dedicated to evaluating the performance of debris-flow barriers based on physical and numerical modeling. The small-scale physical modeling has advantages of being repeatable, but reproducing real debris flows with consideration of proper rheological characteristics and entrainment is a daunting task [7–11]. Numerical approaches have been mainly employed to develop numerical models and software to accurately describe and predict debris-flow behaviors [12–19]. However, relatively less effort has been invested into exploring the influence of barriers on debris-flow characteristics and the interactions between barriers and debris flows [3,20]. Osti and Egashira [20] used sediment–water mixture rheology in 1D flow analysis and reported that check-dam installations could significantly reduce bed erosion, and the farther distance between the two check-dams led to an increase in volume capacity, if two check-dams were installed. Shen et al. [3] used the finite differential method (FDM) based on Voellmy rheology to determine barrier locations that could effectively reduce debris-flow intensity. However, numerical simulation studies on barrier effects with consideration of entrainment, rheological models, and complex 3D terrain are limited, which hampers the understanding and prediction of barrier effects and the design of optimal barrier installations.

This study explored how barrier location affects the characteristics of a debris flow. We chose to model a debris-flow event that occurred at Mt. Woomyeon, Seoul, Korea during heavy rainfall on 26–27 July 2011. The model included the addition of closed-type barriers along the debris-flow channel by simulating a model debris-flow event while varying the installation location from upstream to downstream. The effects of barrier location on debris-flow characteristics were calculated by considering velocity and volume. Moreover, the volumetric capacity (or deposition capacity) of a barrier is an important design factor to reduce overflow-associated risks. Our results shed light on how barriers that are installed to mitigate debris flows affect the various behaviors of such disasters.

## 2. Study Area

The study area is a watershed at Mt. Woomyeon, located in Seoul, South Korea (37°28′14.90″ N and 127°0′21.40″ E; Figure 1a). Mt. Woomyeon is 293 m above sea level at its highest point and is characterized by the abundance of buildings and roads in its vicinity within an area of 5.1 km<sup>2</sup>. On 26–27 July 2011, this mountain was the site of 33 debris flows that were caused by ~150 landslides [5]. The debris flows were triggered on steep slopes (>30°) due to heavy rainfall, the intensity of which is highlighted by the recorded peak rainfall intensity of 112.4 mm/h. The debris flowed at an extremely high velocity (up to 28.6 m/s in the Raemian watershed) due to the high water content and entrainment. Among the many debris flows that took place in Mt. Woomyeon, we chose our reference case (Case REF) as one that flowed along a watershed on the north side of the mountain inundating the Sindonga Apartment Complex. The debris-flow initiation and deposition locations were determined to be 256 m and 70 m above sea level, respectively. The debris-flow path was 627 m in length and the initiation section had an average slope of 26°. The watershed area was 107,200 m<sup>2</sup> [21]. Digital elevation model (DEM) data were acquired before the debris-flow event by the National Geographic Information Institute of Korea [22].

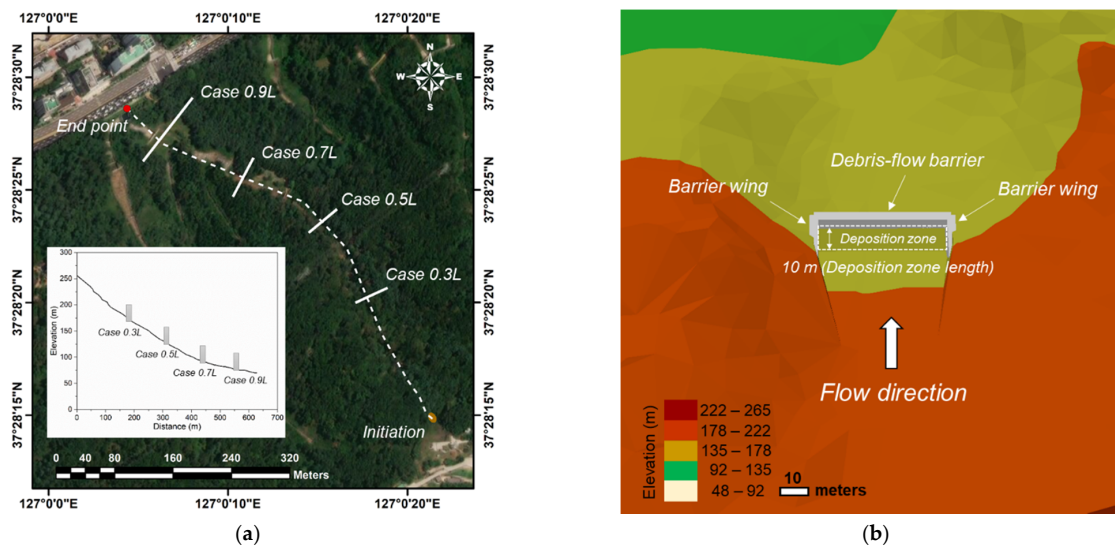


**Figure 1.** Illustration of barrier installations: (a) barrier locations; (b) detailed map view.

### 3. Study Method

#### 3.1. Numerical Code

The commercial software named DAN3D (Dynamic Analysis of Landslides in Three Dimensions) [14,23,24] is an invaluable simulation tool used to examine and study the flow dynamics surrounding viscous debris that possess qualities similar to liquids. DAN3D is based on the smoothed particle hydrodynamics (SPH) method and the equivalent fluid concept, which assumes the multi-phase and multi-component materials of landslides as a single fluid, to interpret the behavior of complex fluids [25]. As changes take place in a complex 3D terrain area, this gives rise to non-hydrostatic and anisotropic internal stresses, which can have significant impacts on landslide dynamics. DAN3D is a semi-empirical method based on physics that uses calibrated input parameters obtained from back-analysis based on real events. The governing equations of DAN3D involve mass and momentum conservation, as follows:

$$\frac{\partial h}{\partial t} + h \left( \frac{\partial v_x}{\partial x} + \frac{\partial v_y}{\partial y} \right) = \frac{\partial b}{\partial t}, \quad (1)$$

$$\rho h \frac{\partial v_x}{\partial t} = \rho h g_x + k_x \sigma_{z(z=b)} \left( -\frac{\partial h}{\partial x} \right) + k_{yx} \sigma_z \left( -\frac{\partial h}{\partial y} \right) + \tau_{zx(z=b)} - \rho v_x \frac{\partial b}{\partial t}, \quad (2)$$

$$\sigma_{z(z=b)} = \rho h \left( g \cos \alpha + \frac{v_x^2}{R} \right) \quad (3)$$

$$\tau_{zx(z=b)} = - \left( \sigma_{z(z=b)} f + \frac{\rho g v_x^2}{\zeta} \right), \text{ and} \quad (4)$$

$$\frac{\partial b}{\partial t} = E_t = E_s h v_x \quad (5)$$

where  $\rho$  is the material bulk density,  $h$  is the bed-normal flow depth,  $\alpha$  is the inclination of the bed from the horizontal position,  $R$  is the bed-normal radius of the curvature of the path in the direction of motion,  $v_x$  is flow velocity in the direction of motion,  $b$  is the bed-normal erosion-entrainment depth, and  $g$  is gravitational acceleration.  $k$  is the stress coefficient, and  $\sigma_z$  and  $\tau_{zx}$  are the bed-normal and basal shear stresses, respectively.  $f$  is the friction coefficient,  $\zeta$  is the turbulence parameter, and  $E_t$  and  $E_s$  are the erosion rates dependent on time and displacement, respectively.

We decided to employ DAN3D due to its following advantages: (a) The code uses complex 3D digital elevation models (DEM) to simulate debris flows. (b) The entrainment process is considered by using an empirical erosion rate based on the momentum transfer between the debris and the bed material. (c) DAN3D can implement five rheological models

(Newtonian, Bingham, Voellmy, plastic, and frictional) to model flow characteristics that are associated with different types of landslides and debris flow. (d) DAN3D is user-friendly and requires relatively little computational resources and time compared to other numerical simulation methods. This advantage was achieved using simplified governing equations and boundary conditions.

### 3.2. Rheological Model

Rheological models play a critical role in describing debris-flow behavior. Specifically, the original purpose of the Voellmy model was to describe snow avalanches [26]; the Voellmy model was implemented to landslide modelling due to the similarities between landslides and snow avalanches in terms of velocity and thickness [23]. The input parameters of the Voellmy model include the frictional coefficient and the turbulence parameter (Equation (4)): the former governs debris-flow deposition properties, whereas the latter influences debris-flow mobility [23]. The frictional coefficient and turbulence parameter are typically determined through back-analysis based on the recorded velocity, run-out distance, and deposited area of the debris flow [12,23,27,28]. Although most debris flow cases in Korea have been reported with high velocities, the debris flow that took place in Mt. Woomyeon exhibited exceptionally rapid velocities of up to 28.6 m/s, as measured from videos taken by residents [5,6], which was a result of heavy rainfall increasing the water content to high levels. Herein, the frictional coefficient and turbulence parameter were set as low and high values, respectively, to recreate the high velocity flows. The input properties and details of the debris-flow event are summarized in Table 1. A field survey noted that most of the debris was deposited downstream near the residential complex. The source volume of the reference case was measured to be approximately 70 m<sup>3</sup> [5]. Back-analysis using the source and deposited debris volumes and deposition area was employed to determine the friction coefficient (0.03), the turbulence parameter (800 m/s<sup>2</sup>), and the erosion rate ( $7.8 \times 10^{-3}$  %/m), as shown in Table 1. The turbulence parameter and the friction coefficient were determined according to ranges employed in previous studies [12].

### 3.3. Barrier Installation

A barrier is created in DAN3D via terrain elevation modifications. Figure 2 illustrates how the DEM was modified to create the barriers. Therefore, barriers would be considered as part of the terrain, and debris flow-barrier interactions are not modeled. A flattened terrain (i.e., deposition zone; Figure 2c,d) is placed at the upstream face of the barrier to reduce the flow velocity and minimize bursting and airborne particles [29]. For further information regarding DAN3D, refer to the papers of McDougall and Hungr [14,24] and McDougall [29]. Four locations were selected for the installation of closed-type barriers to explore how the location of a barrier affects debris-flow behaviors in numerical modeling. In the study site, the distance from the debris source to the road near Sindonga Apartment is 627 m (L), as shown in Figure 1a. For the barrier locations, four points were selected along the debris-flow channel downstream of the initiation location. Accordingly, a barrier was placed at the following locations: 0.3 L (i.e., at a distance of 189 m from the initiation location; Case 0.3 L), 0.5 L (i.e., 311 m distance from the initiation location; Case 0.5 L), 0.7 L (i.e., 437 m distance from the initiation location; Case 0.7 L), and 0.9 L (i.e., 563 m distance from the initiation location; Case 0.9 L). ArcGIS 10.5 was used to create the barriers; a desired shape and size could be achieved by altering the elevations of individual topography grid cells (Figure 2). The direction of each barrier was perpendicular to the direction of the debris flow. In terms of the barrier width, the value was set to be twice the width of the front portion of the simulated debris flow; thus, the barrier was 48 m wide in Case 0.3 L, 50 m in Case 0.5 L, 60 m in Case 0.7 L, and 110 m in Case 0.9 L. The thickness and height of all debris-flow barriers were fixed as 3 m and 7 m, respectively (Table 1). A total of five simulations were conducted: one case did not have any barriers installed (the reference case; Case REF) and the other four included a barrier at their respective locations (Cases

0.3 L to 0.9 L). Table 1 also lists the locations and geometric dimensions of the barriers, in addition to the geotechnical engineering parameters. Geotechnical parameters such as unit weight and internal friction angle were obtained from laboratory tests with soils sampled from the study site.

**Table 1.** Modeling conditions and properties of the debris-flow event and barriers.

|                   |               | Parameters/Cases        | Site                                  |
|-------------------|---------------|-------------------------|---------------------------------------|
| Input parameters  |               | Unit weight             | 16.3 kN/m <sup>3</sup>                |
|                   |               | Internal friction angle | 40°                                   |
|                   |               | Erosion rate            | $7.8 \times 10^{-3}$ %/m              |
|                   |               | Maximum erosion depth   | 1.6 m                                 |
|                   |               | Friction coefficient    | 0.03                                  |
|                   |               | Turbulence parameter    | 800 m/s <sup>2</sup>                  |
| Debris volume     | Source volume | Field                   | 70 m <sup>3</sup>                     |
|                   |               | DAN3D                   | 70 m <sup>3</sup>                     |
|                   | Final volume  | Field                   | 3914 m <sup>3</sup>                   |
|                   |               | DAN3D                   | 4024 m <sup>3</sup>                   |
| Barrier condition |               | Width                   | Distance from the initiation location |
|                   | Case REF      |                         | 627 m                                 |
|                   | Case 0.3 L    | 48 m                    | 189 m                                 |
|                   | Case 0.5 L    | 50 m                    | 311 m                                 |
|                   | Case 0.7 L    | 60 m                    | 437 m                                 |
|                   | Case 0.9 L    | 110 m                   | 563 m                                 |

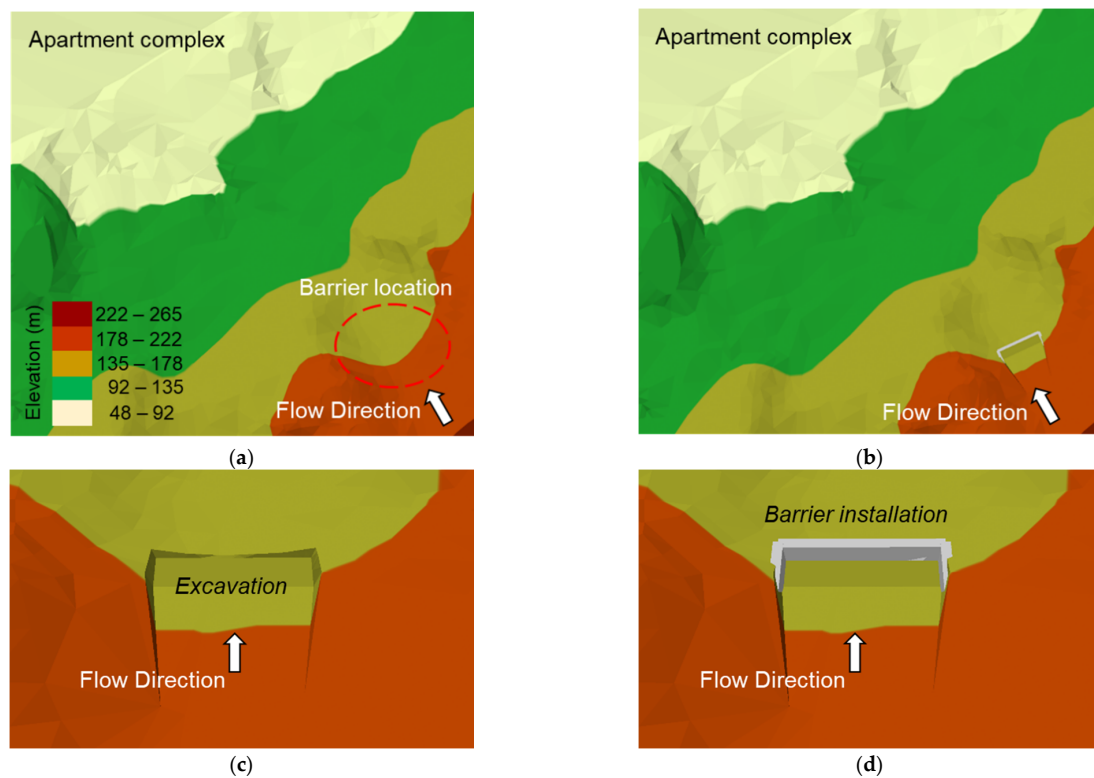


**Figure 2.** Schematics of an installed barrier: (a,c) the elevation model before barrier installation; (b,d) the elevation model after barrier installation.

### 3.4. Deposition Zone at the Upstream Face of a Barrier

The simulated debris flow readily overflows when a barrier is installed on top of the original topography due to the slope of the upstream surface. To correct this, the ground at the upstream face of the barrier was flattened to the lowest elevation. The flattened area is henceforth referred to as the deposition zone. In our simulations, this deposition zone was 10 m in length and equal in width to the barrier. The sharp elevation changes at the cut edges were gently smoothed, and the cell size was kept at 1 m in all numerical simulations. For wide basins that are difficult to block with barriers, the use of barrier shoulders (or wings) on both sides of the barrier is a common solution (Figure 1b). In addition, we set a no-erosion zone near the barrier 50 m in length and width to restrain entrainment around and at the barrier.

## 4. Results and Analysis

From the simulation results, the velocity and volume of the flowing debris and the volume of the deposited debris were computed to evaluate barrier effect. Viscous fluids in the SPH method are modeled as particles, meaning it is possible to track the location, velocity, and volume of each particle over time. In this study, the velocity of the flowing debris was determined using the average velocity value of all particles. The flowing debris and deposited debris volumes were also computed by finding the sum of the volumes of the moving particles and the deposited particles, respectively.

Additionally, we assessed the volumetric parameters of debris flows—the entrained volume  $V_{entrained}$ , the deposited volume  $V_{deposited}$ , and the barrier volumetric capacity  $V_{barrier}$ . The entrained volume  $V_{entrained}$  is the increment in debris volume by entrainment and is determined when all debris come to a halt and/or are trapped. If some debris overflows, the value is determined the moment the overflowed debris enters the urban environment. The total debris-flow volume  $V_{debris}$  is defined as the debris volume passing through a specific barrier location and can also be derived by summing the initial source volume and the entrained volume (i.e.,  $V_{debris} = V_{initial} + V_{entrained}$ ). The volume of deposited debris  $V_{deposited}$  is estimated from the total volume of stationary debris particles (i.e., particles with zero velocity). Lastly, the barrier capacity  $V_{barrier}$  (or the trap capacity of a barrier) is determined based on the barrier height  $H_b$  and width  $W_b$  and is computed as  $V_{barrier} = W_b \cdot H_b^2$ . Herein, it is assumed that the debris is deposited behind the wall with a horizontal-to-vertical slope ratio of 2:1, as suggested in previous experimental studies [9,12,30–34]. As the deposited debris forms a slope near the barrier, the follow-up debris is more likely to overflow over the deposited slope [9,12,30–34]. Accordingly, the retained volume ratio  $R_{ret}$  can be defined as  $R_{ret} = V_{deposited} / V_{debris}$  and be used as an indicator to quantify the trapped debris volume. By comparison, the debris-to-barrier volume ratio  $R_{d/b}$  can be also determined as  $R_{d/b} = V_{debris} / V_{barrier}$ , which represents the volume ratio between the expected total debris volume relative to the barrier's trap capacity.

Figure 3 shows the final debris flow simulation results and Figure 4 shows the debris-flow velocity and volume changes. As shown, the debris-flow velocity rapidly increases to approximately 7 m/s, which is due to the upper flow path having steep slope angles. As the debris flow progresses downslope, its velocity gradually decreases. The sudden drops in velocity take place when the debris collides with each barrier. In Cases 0.3 L and 0.9 L, the debris-flow velocity is reduced to nearly zero, which indicates effective trapping and deposition. By contrast, the results in Cases 0.5 L and 0.7 L reveal that part of the debris continuously flows down after colliding with the barrier, which indicates overflow (Figure 3d,e). This overflowed debris slightly increases in velocity as it traverses down steep slopes downstream of the barriers (Figure 4a), and the volume also increases due to entrainment (Figure 4b). If entrainment effects are ignored, the volume of the overflowed debris would remain constant, whereas the slope of the channel primarily determines the velocity.

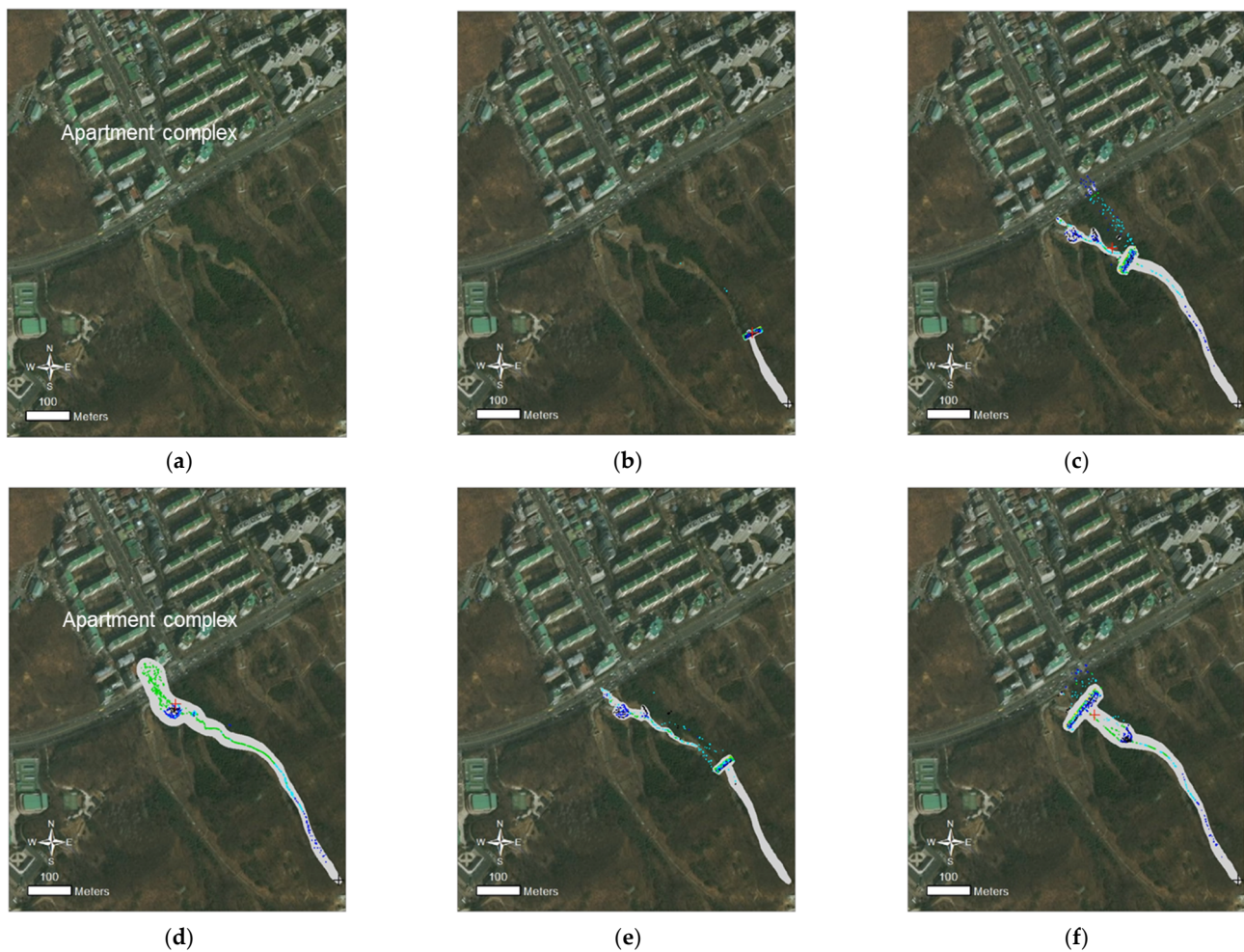


**Figure 3.** Snapshots at the end points of the debris flow simulations: (a) before the event; (b) Case REF; (c) Case 0.3 L; (d) Case 0.5 L; (e) Case 0.7 L; (f) Case 0.9 L.

The debris grows to a volume of  $4100 \text{ m}^3$  as it approaches the downstream roadway at 85 s in Case REF (Figure 4b). In contrast, none of the cases with installed barriers exhibited debris volumes higher than  $1000 \text{ m}^3$ . In particular, in Case 0.3 L the retained volume ratio  $R_{ret}$  is unity, and the deposited volume is equal to the total debris volume (Figure 4b,c). This indicates zero overflow as the barrier completely traps and deposits all debris. This completed trapping by the barrier in Case 0.3 L can be readily expected with debris-to-barrier volume ratios  $R_{d/b}$  far less than 0.5. Figure 5a illustrates how debris deposits near a barrier without overflow. The debris depth near the barrier is less than 1 m, which is lower than the height of the wall (5 m), as shown in Figure 5.

The further downstream the barrier is located, the greater its size due to the increased channel width. Therefore, the deposited debris volume increases as the distance between the barrier location and the initiation (or source) location increases (e.g.,  $230 \text{ m}^3$  for Case 0.3 L,  $450 \text{ m}^3$  for Case 0.5 L,  $1350 \text{ m}^3$  for Case 0.7 L, and  $3620 \text{ m}^3$  for Case 0.9 L, as shown in Figure 4b). For Cases 0.5 L, 0.7 L, and 0.9 L, the difference between the barrier capacity and the total debris volume is minimal, with the former being even smaller than the latter in cases 0.7 L and 0.9 L (Figure 4c); therefore, the debris-to-barrier volume ratios  $R_{d/b}$  are greater than 0.8 (Figure 4d). As expected, overflow occurs in these cases as the retained volume ratios  $R_{ret}$  are less than 1 [12].

The results imply that a barrier could be installed near the initiation location to reduce the size of the barrier and effectively capture the debris before entrainment effects take place to increase the debris volume. These results are consistent with findings in previous studies [3,12,35]. In addition, it was found that a barrier with a  $R_{d/b}$  of less than 0.7

could trap debris without overflowing. However, it is worth noting that the prediction of exact initiation locations and the volume of landslides and debris flows still remain as challenging tasks.

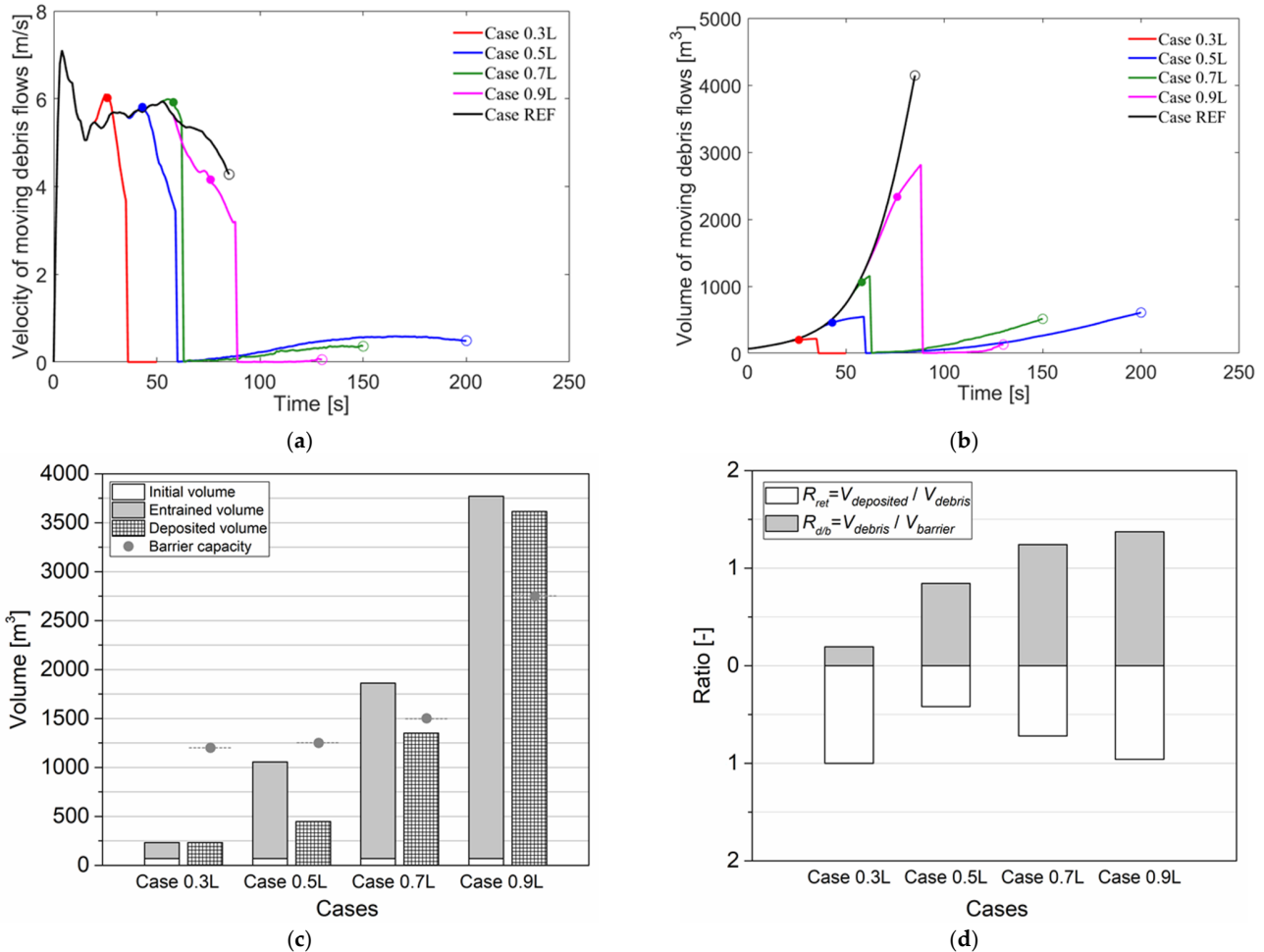


**Figure 4.** Effect of barrier installation on characteristics of the debris flow: (a) the debris-flow velocity; (b) the deposited volume behind the barrier; (c) the volumetric characteristics of debris flows with respect to barrier location and capacity; (d) the retained volume ratio ( $R_{ret}$ ) and the debris-to-barrier volume ratio ( $R_{d/b}$ ). Note that the filled and empty circles indicate the time when the debris flow made contact with each barrier and the village, respectively.

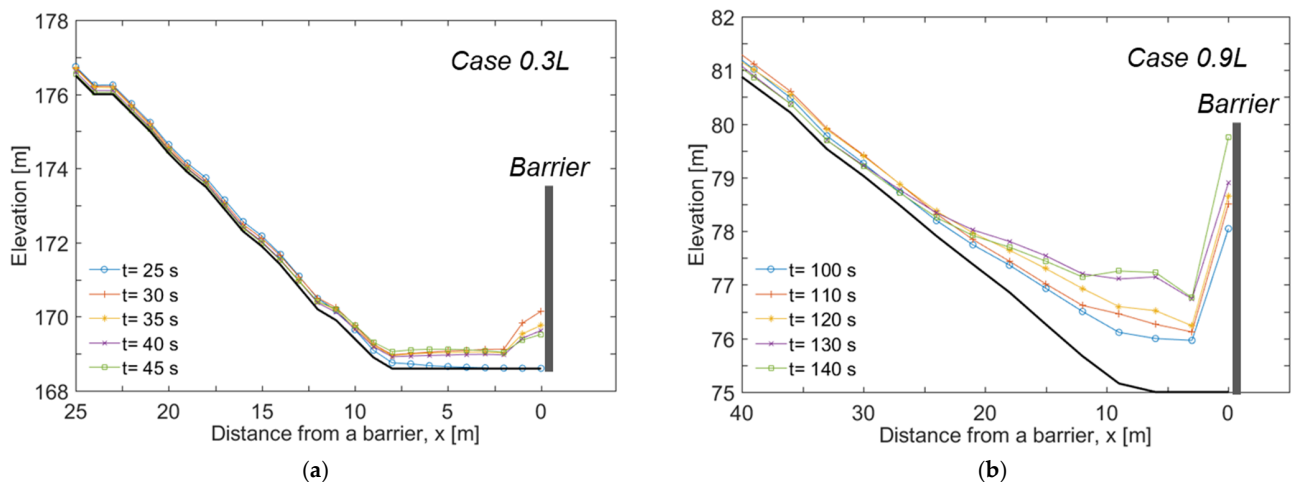


**Figure 5.** Debris depths near the vicinity of a barrier: (a) Case 0.3 L with no overflow and (b) Case 0.9 L with overflow.

## 5. Discussion and Implication

The implications and limitations of our numerical approach can be described as follows. (a) 3D terrain morphologies of greater complexity could be implemented to take the depositional characteristics of debris flows into further consideration. In addition to colliding with barriers, debris can bounce backwards, or slide to the side of barriers and also interact with the terrain [36]. (b) It may be insightful to perform similar simulations with various types of barriers, such as closed-type or open-type barriers, or drainage paths. This can be achieved using 3D digital elevation maps (DEM) by altering the cell size. However, modifying the cell size in an SPH model can drastically influence the interactions between the SPH particles (debris materials), barriers, and the terrain. (c) Considering the impact of entrainment effects on debris flows [3,12,37,38], future studies should focus on how entrainment influences the rise in debris-flow volume or risk overestimating the performance of debris-flow barriers. (d) The rheology of a debris flow is an important factor as it determines the velocity of a debris flow, in addition to how it deposits. Given that the presented method is centered around the parameters and terrain of a particular site, the approach may need to be adjusted when being applied to other locations. (e) The barriers in the presented approach were implemented by modifying the terrain morphology; thus, they are considered as part of the terrain instead of structural elements, preventing the direct assessment of barrier structural stability. We recommend using the presented SPH-based approach to derive debris-flow characteristics (e.g., depth, velocity, and volume) that can be used as inputs for a separate structural analysis [39,40].

## 6. Conclusions

This study investigated how the location of a barrier along a channel affects debris-flow behavior based on numerical simulations using DAN3D. Entrainment causes a rise in debris volume proportional to the source-to-barrier distance. At the same time, the basin width increases further downstream. As expected, barriers installed at locations further downstream need to be larger than barriers installed upstream. Furthermore, our results revealed that debris can partially flow over a barrier if the debris volume is greater than the deposition capacity of the barrier. The overflowed debris was observed to increase in flow velocity and volume due to steep slopes beyond the barrier. This overflowed debris can continually flow further down and result in additional damage to areas downstream. Therefore, barriers could be installed nearer to debris-flow initiation locations as it is more beneficial and effective from the perspectives of barrier size and overflow mitigation. This is because barriers in such locations can restrain the entrainment-driven growth of debris flow in the early stages of run-out. However, it is worth pointing out that there are often some technical and economic challenges associated with barrier installation at upstream locations, such as road accessibility and maintenance costs. Therefore, barrier locations need to be carefully determined to ensure optimal debris-flow barrier designs that are effective and efficient. In addition to analyzing the movement of debris flows, DAN3D is also capable of identifying changes in debris flow characteristics due to the installation of barriers. Therefore, the numerical software is a useful tool when designing barriers as it can analyze the debris flow reduction effects according to the dimensions and location of barriers prior to installation.

**Author Contributions:** Conceptualization, S.-K.C. and T.-H.K.; numerical analysis, S.-K.C.; analysis of data, writing, review and editing, S.-K.C. and T.-H.K.; supervision, T.-H.K. All authors have read and agreed to the published version of the manuscript.

**Funding:** This work was financially supported by Korea Ministry of Land, Infrastructure and Transport (MOLIT) as Innovative Talent Education Program for Smart City, and also supported by the National Research Foundation of Korea (NRF) grant funded by the Korea government (MSIT) (No. 2021R1A2C4002358).

**Data Availability Statement:** The data presented in this study are available on request from the corresponding author.

**Conflicts of Interest:** The authors declare no conflict of interest.

## References

1. Jakob, M.; Hungr, O. *Debris Flow Hazards and Related Phenomena*; Springer: Berlin/Heidelberg, Germany, 2005.
2. Tang, C.; Zhu, J.; Chang, M.; Ding, J.; Qi, X. An empirical–statistical model for predicting debris flow run-out zones in the Wenchuan earthquake area. *Quat. Int.* **2012**, *250*, 63–73. [[CrossRef](#)]
3. Shen, W.; Wang, D.; Qu, H.; Li, T. The effect of check dams on the dynamic and bed entrainment processes of debris flows. *Landslides* **2019**, *16*, 2201–2217. [[CrossRef](#)]
4. Orense, R.P.; Sapuay, S.E. Preliminary report on the 17 February 2006 Leyte, Philippines landslide. *Soils Found.* **2006**, *46*, 685–693. [[CrossRef](#)]
5. Yune, C.Y.; Chae, Y.K.; Paik, J.; Kim, G.; Lee, S.W.; Seo, H.S. Debris flow in metropolitan area—2011 Seoul debris flow. *J. Mt. Sci.* **2013**, *10*, 199–206. [[CrossRef](#)]
6. Jeong, S.; Kim, Y.; Lee, J.K.; Kim, J. The 27 July 2011 debris flows at Umyeonsan, Seoul, Korea. *Landslides* **2015**, *12*, 799–813. [[CrossRef](#)]
7. Wenbing, H.; Guoqiang, O. Efficiency of slit dam prevention against non-viscous debris flow. *Wuhan Univ. J. Nat. Sci.* **2006**, *11*, 865–869. [[CrossRef](#)]
8. Kim, Y.; Nakagawa, H.; Kawaike, K.; Zhang, H. *Study on Characteristic Analysis of Closed-Type Sabo Dam with a Flap due to Dynamic Force of Debris Flow*; Kyoto University: Kyoto, Japan, 2013; pp. 503–522.
9. Ng, C.W.; Choi, C.; Song, D.; Kwan, J.; Koo, R.; Shiu, H.; Ho, K.K. Physical modeling of baffles influence on landslide debris mobility. *Landslides* **2015**, *12*, 1–18. [[CrossRef](#)]
10. Wendeler, C.; Volkwein, A. Laboratory tests for the optimization of mesh size for flexible debris-flow barriers. *Nat. Hazards Earth Syst. Sci.* **2015**, *15*, 2597–2604. [[CrossRef](#)]
11. Choi, S.K.; Lee, J.M.; Kwon, T.H. Effect of slit-type barrier on characteristics of water-dominant debris flows: Small-scale physical modeling. *Landslides* **2018**, *15*, 111–122. [[CrossRef](#)]
12. Choi, S.K.; Park, J.Y.; Lee, D.H.; Lee, S.R.; Kim, Y.T.; Kwon, T.H. Assessment of barrier location effect on debris flow based on smoothed particle hydrodynamics (SPH) simulation on 3D terrains. *Landslides* **2021**, *18*, 217–234. [[CrossRef](#)]
13. O'Brien, J.S.; Julien, P.Y.; Fullerton, W.T. Two-dimensional water flood and mudflow simulation. *J. Hydraul. Eng.* **1993**, *119*, 244–261. [[CrossRef](#)]
14. McDougall, S.; Hungr, O. A model for the analysis of rapid landslide motion across three-dimensional terrain. *Can. Geotech. J.* **2004**, *41*, 1084–1097. [[CrossRef](#)]
15. Pirulli, M.; Mangeney, A. Results of back-analysis of the propagation of rock avalanches as a function of the assumed rheology. *Rock Mech. Rock Eng.* **2008**, *41*, 59–84. [[CrossRef](#)]
16. Beguería, S.; Van Asch, T.W.; Malet, J.P.; Gröndahl, S. A GIS-based numerical model for simulating the kinematics of mud and debris flows over complex terrain. *Nat. Hazards Earth Syst. Sci.* **2009**, *9*, 1897–1909. [[CrossRef](#)]
17. Pastor, M.; Haddad, B.; Sorbino, G.; Cuomo, S.; Drempetic, V. A depth-integrated, coupled SPH model for flow-like landslides and related phenomena. *Int. J. Numer. Anal. Methods Geomech.* **2009**, *33*, 143–172. [[CrossRef](#)]
18. Christen, M.; Kowalski, J.; Bartelt, P. RAMMS: Numerical simulation of dense snow avalanches in three-dimensional terrain. *Cold Reg. Sci. Technol.* **2010**, *63*, 1–14. [[CrossRef](#)]
19. Quan, L. Dynamic Numerical Run-Out Modeling for Quantitative Landslide Risk Assessment. Ph.D. Thesis, University of Twente, Enschede, The Netherlands, 2012.
20. Osti, R.; Egashira, S. Method to improve the mitigative effectiveness of a series of check dams against debris flows. *Hydrol. Process. Int. J.* **2008**, *22*, 4986–4996. [[CrossRef](#)]
21. Korean Society of Civil Engineers (KSCE). *Research Contract Report: Causes Survey and Restoration Work of Mt. Woomyeon Landslide*; Korean Society of Civil Engineers: Seoul, Korea, 2012.
22. National Geographic Information Institute of Korea (NGII). *Digital Elevation Maps of South Jeolla Province with the Scale of 1:5000*; National Geographic Information Institute of Korea: Suwon, Korea, 2010.
23. McDougall, S. 2014 Canadian Geotechnical Colloquium: Landslide runout analysis—Current practice and challenges. *Can. Geotech. J.* **2017**, *54*, 605–620. [[CrossRef](#)]
24. McDougall, S.; Hungr, O. Dynamic modelling of entrainment in rapid landslides. *Can. Geotech. J.* **2005**, *42*, 1437–1448. [[CrossRef](#)]
25. Hungr, O. A model for the run-out analysis of rapid flow slides, debris flows, and avalanches. *Can. Geotech. J.* **1995**, *32*, 610–623. [[CrossRef](#)]
26. Voellmy, A. Über die Zerstörungskraft von Lawinen. *Schweiz. Bauztg.* **1955**, *73*, 212–285.
27. Cepeda, J.; Chávez, J.A.; Martínez, C.C. Procedure for the selection of runout model parameters from landslide back-analyses: Application to the Metropolitan Area of San Salvador, El Salvador. *Landslides* **2010**, *7*, 105–116. [[CrossRef](#)]
28. Aaron, J.; McDougall, S.; Nolde, N. Two methodologies to calibrate landslide runout models. *Landslides* **2019**, *16*, 907–920. [[CrossRef](#)]
29. McDougall, S. A New Continuum Dynamic Model for the Analysis of Extremely Rapid Landslide Motion across Complex 3D Terrain. Ph.D. Thesis, University of British Columbia, Vancouver, BC, Canada, 2006.

30. Ng, C.W.W.; Choi, C.E.; Kwan, J.S.H.; Koo, R.C.H.; Shiu, H.Y.K.; Ho, K.K.S. Effects of baffle transverse blockage on landslide debris impedance. *Procedia Earth Planet. Sci.* **2014**, *9*, 3–13. [[CrossRef](#)]
31. Zhou, G.G.D.; Song, D.; Choi, C.E.; Pasuto, A.; Sun, Q.C.; Dai, D.F. Surge impact behavior of granular flows: Effects of water content. *Landslides* **2018**, *15*, 695–709. [[CrossRef](#)]
32. Song, D.; Choi, C.E.; Ng, C.W.W.; Zhou, G.G.; Kwan, J.S.; Sze, H.Y.; Zheng, Y. Load-attenuation mechanisms of flexible barrier subjected to bouldery debris flow impact. *Landslides* **2019**, *16*, 2321–2334. [[CrossRef](#)]
33. Siyou, X.; Lijun, S.; Yuanjun, J.; Xin, Q.; Min, X.; Xiaobo, H.; Zhenyu, L. Experimental investigation on the impact force of the dry granular flow against a flexible barrier. *Landslides* **2020**, *17*, 1465–1483. [[CrossRef](#)]
34. Tan, D.Y.; Yin, J.H.; Qin, J.Q.; Zhu, Z.H.; Feng, W.Q. Experimental study on impact and deposition behaviours of multiple surges of channelized debris flow on a flexible barrier. *Landslides* **2020**, *17*, 1577–1589. [[CrossRef](#)]
35. Remaître, A.; Van Asch, T.W.; Malet, J.P.; Maquaire, O. Influence of check dams on debris-flow run-out intensity. *Nat. Hazards Earth Syst. Sci.* **2008**, *8*, 1403–1416. [[CrossRef](#)]
36. Iverson, R.M.; George, D.L.; Logan, M. Debris flow runup on vertical barriers and adverse slopes. *J. Geophys. Res. Earth Surf.* **2016**, *121*, 2333–2357. [[CrossRef](#)]
37. Revellino, P.; Hungr, O.; Guadagno, F.M.; Evans, S.G. Velocity and runout simulation of destructive debris flows and debris avalanches in pyroclastic deposits, Campania region, Italy. *Environ. Geol.* **2004**, *45*, 295–311. [[CrossRef](#)]
38. Hungr, O.; Evans, S.G. Entrainment of debris in rock avalanches: An analysis of a long run-out mechanism. *Geol. Soc. Am. Bull.* **2004**, *116*, 1240–1252. [[CrossRef](#)]
39. Dai, Z.; Huang, Y.; Cheng, H.; Xu, Q. SPH model for fluid–structure interaction and its application to debris flow impact estimation. *Landslides* **2017**, *14*, 917–928. [[CrossRef](#)]
40. Chen, H.X.; Li, J.; Feng, S.J.; Gao, H.Y.; Zhang, D.M. Simulation of interactions between debris flow and check dams on three-dimensional terrain. *Eng. Geol.* **2019**, *251*, 48–62. [[CrossRef](#)]